NANO LETTERS

2007
Vol. 7, No. 6
1736−1740

Two Particle Enhanced Nano Raman Microscopy and Spectroscopy

Phillip Olk,* Jan Renger, Thomas Härtling, Marc Tobias Wenzel, and Lukas M. Eng

Institut für Angewandte Photophysik, TU Dresden, 01062 Dresden, Germany

Received March 28, 2007; Revised Manuscript Received April 23, 2007

ABSTRACT

The distance- and polarization-dependent near-field enhancement of two coupling metal nanoparticles (MNPs) is analyzed by means of the novel scanning particle enhanced Raman spectroscopy (SPRM) technique. In contrast to single MNP Raman experiments, the near-field coupling between two dissimilar MNPs as followed here leads to a Raman hot spot yielding an extra enhancement factor of 17.6 and 20, as proven here both in experiment and in theory. Three-dimensional electric field calculations for our two-particle arrangements were performed using the semianalytical multiple-multipole method. An excellent agreement is found to our experiments, in which we inspect the interaction between a "scanning" 30 nm gold MNP (Au30) and a "fixed" 80 nm Au MNP (Au80). The Au80 MNP is attached to the apex of an optical fiber manipulator and exposed to the Gaussian focus of a high NA = 1.45 objective at $\lambda = 532$ nm. A monolayer of 1-octanethiol molecules covering the Au80 MNP serves as the electric field prober when scanning the Au30 MNP through the optical focus. This constellation allows recording the Raman signatures from a very low number of well-confined molecules. Moreover, also the spectral and spatial dependence could be explored with a superb sensitivity and very low integration time.

The optical near-field[1] of single spherical metallic nanoparticles (MNPs) is well suited for Raman[2] and fluorescence[3] excitation at enhanced local electric fields, aiming toward the single molecular analysis.[4] If properly attached to a scanning probe tip, single MNPs are ideal to be used as well-confined scattering objects showing practical use for instance in (scattering) scanning near-field optical microscopy (SNOM).[5,6]

We apply here the optical properties of such a tip−particle system to extend scanning particle enhanced Raman microscopy (SPRM) toward two particle enhanced nano Raman microscopy and spectroscopy. While sharing similarities to tip enhanced Raman spectroscopy (TERS), the metal-coated tip[7,8] is replaced here by a single MNP attached to an optical fiber's apex. Benefits of such a spherical MNP probe are its low intrinsic degree of polarization dependence and the well-localized field enhancement due to the smallness of the MNP. Furthermore, energetic losses due to excitation of surface plasmon polaritons in solid metal tips[9] are eliminated.

When two MNPs are placed a short distance apart, they interact by means of near-field coupling for light of appropriate polarization.[10−13] This coupling manifests in a strong field enhancement between the two MNPs. Additionally, the two individual plasmon resonances of the MNPs are re-formed to one effective (red- or blue-shifted) resonance.[13,14] The precise spectral properties of the new plasmon resonance are subject to the MNPs material, shape, size, orientation, and surrounding medium and the characteristics of the incident light beam such as polarization and intensity distribution.[13−18] The highly localized and enhanced electromagnetic fields between two particles may be used, e.g., for improved generation of Raman signals[19,20] and surface plasmon amplification.[21,22] Note that for certain combinations involving three and four MNPs, hot spots with more than a 1000-fold intensity compared to the incident light have been predicted theoretically.[18,23]

In this Letter, we limit the system under examination to consist of two gold metal nanoparticles only, with the first and second MNP measuring 80 nm (Au80) and 30 nm (Au30) in diameter, respectively (all MNPs obtained from British Biocell International Ltd., Great Britain). Individual MNPs are routinely inspected for their optical quality by recording spectra under white light illumination. The typical spectral scattering cross section σ of an Au80 and Au30 MNP recorded in immersion oil ($n = 1.52$) is shown in Figure 1a.

The Au80 is attached to the apex of a tapered optical fiber serving as a single particle manipulator following the recipe as described in ref 5, using APTMS (13822-56-5, Sigma-Aldrich Chemie GmbH, Germany) as the bifunctional interlinking molecule to attach the Au80 to the glass fiber. The fiber is mounted to a quartz tuning fork which serves as a distance-sensitive feedback control[3] similar to scanning near-field optical microscopy.[24] (Note that the fiber itself simply acts as the MNP manipulator and is not used here for any optical purposes.)

* Corresponding author. E-mail: polk@iapp.de. Web: http://iapp.de.

10.1021/nl070727m CCC: $37.00
Published on Web 05/11/2007

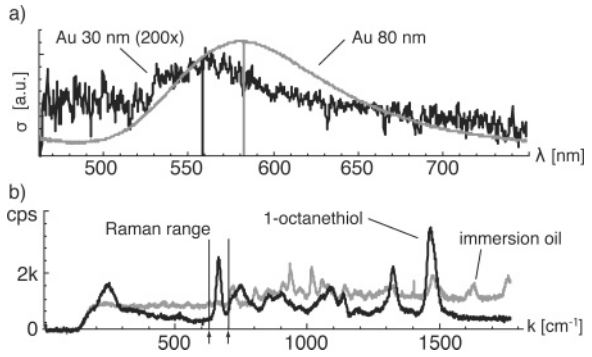

Figure 1. (a) Measured white light scattering efficiency σ of single gold nanoparticles in immersion ($n = 1.52$), having a diameter of 30 nm (Au30) and 80 nm (Au80). The peak positions (at 560 and 580 nm, respectively) allow concluding on the particle diameter. As the scattering cross sections are proportional to the square of the particle volume, the recordable intensities differ by a factor of ≈350. Anomalously shaped particles or pairs of particles would result in a broadened peak or even several spectral features. (b) Raman spectra of pure immersion oil and 1-octanethiol (AT), with the latter bound to the 80 nm gold sphere. Near-field analysis takes place at the designated spectral range (see arrows) between 630 and 700 cm^{-1}. This can be assigned to the ν(S−C)T stretching. The height of this peak serves as the reference Raman signal per unit time.

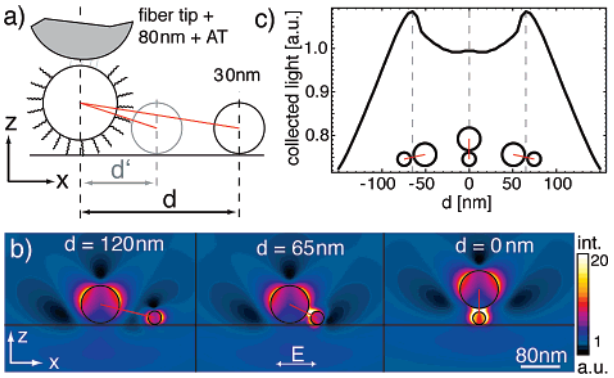

Figure 2. (a) Cartoon of the system under examination. An 80 nm gold particle (Au80) is attached to a fiber tip by means of APTMS. The particle is then coated with a molecular monolayer with known Raman signature. While this particle is kept in the optical focus, a second particle of Au30 is approached. The red lines indicate the connection of the two sphere centers (the structure's principal axis) for two different distances d and d'. Note the change of its relative direction with respect to the polarization. (b) Calculated intensity distribution of the described scenario. Red lines represent the two MNPs' principal axis. For $|d| = 65$ nm, a local intensity enhancement of $F_{MMP} \approx 20\times$ is expected. See video in Supporting Information. (c) Calculated distance dependence of the intensity that is backscattered into a cone of 144° opening angle.

After the Au80 MNP is attached to the fiber, the MNP is coated with a self-assembled monolayer of 1-octanethiol (111-88-6, ABCR GmbH & Co. KG, Germany) by submerging the tip into the alkanethiol (AT) for 15 min. Extensive rinsing with ethanol removes residual AT that did not bind to the gold surface, resulting in a monolayer coverage of the Au80 MNP with AT molecules. The Raman spectrum of these AT molecules is shown in Figure 1b producing a strong peak at 680 cm^{-1}. This peak can be assigned to the ν(C−S)T oscillation of the molecule.[25−27]

The Au80 MNP is exposed to the focus of a high numerical aperture objective (Zeiss α-Planfluar, NA = 1.45) which is mounted on an inverted optical microscope (Zeiss Axiovert 200). Since all AT molecules are firmly restricted to the Au80 surface and the Raman signature is known, they provide key access to the near-field enhancement that is probed in our two-particle SPRM experiment.

In order to couple two MNPs, we spin-coat Au30 MNPs onto a glass cover slip with an interparticle distance being larger than 10 μm. The sample is introduced into the inverted optical setup and covered by a immersion liquid matching the substrate's index of refraction. This suppresses effects from the substrate−air interface and the fiber tip. The Au30 MNPs are inspected for their scattering signature with the Au80 tip being retracted. The typical Au30 scattering spectrum σ recorded in immersion oil is shown in Figure 1a. Now, the coated Au80 tip is brought back into the focus and kept at this position by means of a sensitive shear force feedback[28] operated at an oscillation amplitude of 2 nm. Note that in our setup, the sample (Au30 MNPs) is always scanned under the fixed Au80 tip.

The electric field distribution in the vicinity of such a two-particle system was calculated at first for an excitation wavelength of $\lambda = 532$ nm by means of the multiple multipole (MMP) method.[29−31] For a fixed Au80 MNP at x, y, $z = 0$, the distance d parallel to the x coordinate (see Figure 2a) was varied in steps of 5 nm, ranging from 150 to 0 nm. For interparticle distances larger than 120 nm, the Au80 and Au30 act as quasi-independent scatterers since their near-field interaction is weak (see Figure 2b, left).

When d is reduced from 120 nm toward 0 nm, the electric field between the MNPs is drastically enhanced, as indicated by the bright color in Figure 2b. The enhancement magnitude is determined by the minimum distance between the two MNPs—here, the surface−surface distance is assumed to measure approximately 3 nm. This value results from the AT layer thickness (≈1 nm) and 2 nm tip oscillation amplitude reported above as needed for shear-force feedback operation. A maximum intensity enhancement of $F_{MMP} \approx 20$ is reached for $d \approx 65$ nm (see Figure 2b, center). When d is further reduced to $d = 0$, the shear-force controller lifts the Au80 tip in order to follow the Au30 topography on the glass sample (see Figure 2b, right).

When comparing our experimental investigations of the two-particle SPRM to these calculations, we face two obstacles. The first experimental peculiarity concerns the spatial shaping of the exciting laser beam at $\lambda = 532$ nm: while the field calculations in Figure 2b assumed a plane wave excitation, the focal region has a Gaussian intensity distribution with a fwhm of 230 nm, as measured experimentally. The second fact to keep in mind is that the Raman signal is collected under a 180° configuration (reflected-light setup type) using the whole detection cone of 144° full angle aperture (NA = 1.45). Only light radiated into this cone can add to the measured Raman signal.

To comply for these peculiarities, further calculations were undertaken: the d-dependent amount of light, backscattered from the Au80 surface *and* radiated into the detection cone

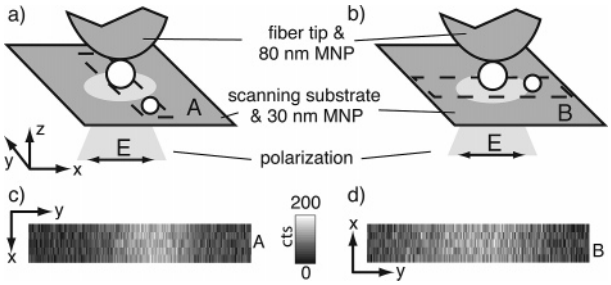

Figure 3. (a) Sketch of the experimental setup. Au80 persists in the laser focus, whereas the substrate carrying Au30 is scanned across. All measurements take place in immersion. In configuration A, the Au30 approaches the focus along the *y* axis; hence the two MNPs' principal axis is perpendicular to the polarization direction of the excitation, which is aligned parallel to *x*. The Raman signal is increased due to the enlarged scattering cross section. In configuration B, the *same* Au30 is approached toward the Au80 along the *x* axis, in parallel to *E*, permitting coupling-induced near-field enhancement. The Raman-scattered light is collected by the illumination optics, separated from the excitation light by a notch filter, fed into a spectrometer, and mapped into a two-dimensional plot. (c) Scanned area's intensity map for configuration A. (d) Intensity map for configuration B. The scanned areas are 20 × 1000 nm (5 × 250 pixels) in size. Note the warped aspect ratios for the sake of clarity.

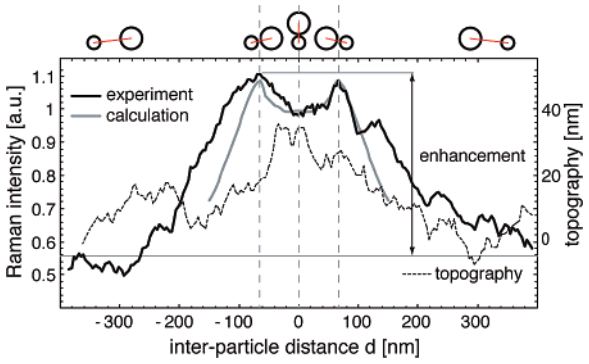

Figure 4. Raman intensity from a hot spot between two MNPs, displaying both calculation and experimental data with the latter averaged over three sets of A and B measurements with different Au30. While Au80 is always kept in focus, Au30 is scanned across the focal region. For large $|d| > 300$ nm, the Raman signal stems from a virtually isolated Au80 MNP. At a small distance *d*, strong near-field coupling between the two MNPs causes an increase of the Raman signal from ≈0.55 to 1.1 (in arbitrary units), hence by a factor of ≈2. The topography height corresponds to an Au80, which is scanned across an Au30.

was calculated vectorially rather than scalarly. This Au80-surface-specific scattering cross section of the two MNPs is then weighted by the spatial intensity distribution of the excitation light, leading to a distance dependence of the light stemming from the AT-coated Au80 surface as illustrated in Figure 2c.

The local dip in the intensity distribution in this figure is expected for $d = 0$. Furthermore, we intuitively would expect an intensity maximum whenever the separation between the two MNPs is minimal. (The two MNPs "touch" at $|d'| = 51$ nm, maintaining a minimum surface separation of 3 nm as demanded by the AT layer (≈1 nm) and the oscillation amplitude (≈2 nm) necessary to provide shear-force feedback.) However, as seen from Figure 2c, the actual intensity maximum is theoretically predicted for a slightly larger distance $|d|$, which is owed to the fact that the two MNPs are in contact to the substrate: the closer they get, the larger becomes the misalignment of the structure's principal axis and the polarization. This tradeoff between distance and alignment results in an optimum at 65 nm for the relative distance *d* between the two MNPs.

The local field enhancement of the coupled, but geometrically nonsymmetric, structure is very sensitive to the relative alignment of the incident light polarization. It is therefore mandatory to inspect our two-particle system in different relative arrangements as sketched in Figure 3. Two cases are considered here:

Case A. For light being polarized perpendicularly to the two MNPs' principal axis (see Figure 3a), an enhancement can be recorded if the Au30 enters into the focal region; the second MNP increases the structure's overall scattering cross section, causing a severe increase in the Raman signal although no strong near-field coupling of the MNPs takes place.

Case B. When the projected principal axis between the two MNPs is aligned in parallel to the polarization vector of the incident light beam (see Figure 3b) an enhanced Raman signal is recorded as well. This signal, however, consists of two components; as for case A, the overall scattering cross section of the structure in the focal region is increased. Additionally, a significant near-field coupling takes place, producing a Raman hot spot.

In order to isolate the coupling-enhanced Raman signatures from the increased signal caused by scattering, the two signals (cases A and B) have to be subtracted (B − A). This results in evaluating the net contribution to the Raman signal dominated by the plasmon coupling.

The distance-dependent, coupling-mediated Raman enhancement (averaged over three different Au30 MNPs) is displayed in Figure 4. On comparison of the measured data to the upshots from our calculations, the following key features are retrieved: at $|d| = 0$, the Raman intensity indicates a local minimum. The positions of the two maxima determined by the given geometry are in good agreement with our calculations, being at distances $|d| = 65$ nm. Their height (1.1-fold relative to the local minimum) is in good agreement with our calculation as well. For larger $|d|$, solely the nonenhanced Raman signal of the remaining Au80 is collected.

In order to quantify the local hot spot and the benefit of utilizing two-particle coupling, we take a closer look at the retrieved data. Treating the Raman signal of the singled AT-covered Au80 as being the reference signal intensity S_{ref}, the Au30-mediated overall Raman intensity I' can be determined from Figure 4 to be $I' = RS_{ref} \approx 2S_{ref}$, with $R \approx 2$ being the overall enhancement factor of the Raman signal. Subscript ref denotes the properties of the bare Au80 concerning field and quantity of molecules serving as the reference, while index HS is for the contributors to the additional enhancement by the hot spot. Assuming a molecular density[32] of four molecules per square nanometer,

we claim that the normal intensity S_{ref} stems from about a third of the surface-bound AT molecules, so $z_{ref} \approx 27000$ molecules. As the proximity of an Au30 approximately doubles the signal to $S' = 2S_{ref} \approx S_{ref} + S_{HS}$, we conclude that $S_{ref} \approx S_{HS}$, with S_{HS} being the additional Raman intensity stemming from the two-MNP-induced hot spot. From our calculations (see Figure 2b) we estimate the hot spot surface section to an equivalent circular area projected onto the Au80 surface measuring 15 nm in diameter, which results in an extra contribution to S_{HS} of less than 1% of all molecules (i.e., $z_{HS} \approx 5700$ at most). Although involving only very few molecules, the signal is sufficiently strong for recording scanned images (see Figure 3c). This fact alone demonstrates the high performance of the two-particle SPRM, especially when considering the spectral fanning and the short experimental integration time of 0.2 s per pixel only (incident power 2 mW).

The hot spot's average intensity can be estimated as follows: As the Raman signal is approximately doubled by the Au30, we write $S_{ref} \approx S_{HS}$. (The intensity of a Raman signal S depends on the illumination intensity in the following way: $S \propto I^2$.) In turn, the illuminating intensity I depends on the electric field E: $I \propto |E|^2$. We assume that each Raman component is generated by a number of molecules z which are exposed to a certain electric field intensity I: $z_{ref}I_{ref}^2 = z_{HS}I_{HS}^2$.

Introducing the Au30 results in an intensity enhancement by a factor of F, i.e., $z_{ref}I_{ref}^2 = z_{HS}I_{HS}^2 = z_{HS}(FI_{ref})^2$, giving $F = (z_{ref}/z_{HS})^{1/2}$. This leads to an intensity enhancement at the hot spot of $F \approx 2.2$ with respect to the background Raman signal. Since this background signal is generated by an Au80-type MNP which already possesses an enhanced near-field intensity of $F_{80} \approx 8$,[18] we find a maximum experimental enhancement factor F_{max} for the given hot spot structure of $F_{max} = FF_{80} \approx 17.6$ with respect to the illumination intensity.

Theoretically, an enhancement by a factor of $F_{MMP} \approx 20$ was calculated for the structure under examination as shown in Figure 2b. The discrepancy between F_{max} and F_{MMP} can be eased by two experimental requirements which differ slightly from the assumptions made in our calculations. One constraint was the constant gap width of 3 nm between the two MNPs, which might be erroneous since the tip oscillates at a 2 nm amplitude in our experiments, yielding an overall average <3 nm. A second measure in order to simplify calculations was the assumption of a weighted plane wave excitation, which is in contrast to the experimental Gaussian beam causing a more complicated light−particle interaction.[33] Moreover, it is also these intrinsic imperfections of focused light that are relevant for the deviations between calculation and experiment for intermediate distances 120 nm $< |d| <$ 200 nm (see Figure 4).

As the applicability of SPRM is well proven here, we may now consider other MNP configurations being tuned to either higher spatial resolution or stronger signal intensities. The latter can be achieved for the system used here by changing the excitation wavelength to be closer to the (Au80-dominated) plasma resonance of the coupling MNPs and by a smaller deviation between the principal axis and the excitation's polarization. If these two conditions are optimized, we expect a field intensity enhancement in air[18] of $F_{opt} = 1000$ instead of $F_{MMP} = 20$. The efforts in reaching smaller MNP diameters in order to enhance the spatial resolution for microscopy and spectroscopy have to be counterbalanced by the dramatically reduced local field enhancement for decreasing MNP diameters: two particles of, e.g., 30 and 10 nm in diameter yield a calculated maximum signal enhancement of $F'_{MMP} = 10$ only, in comparison to $F_{MMP} = 20$ calculated here.[18] A triple MNP arrangement could possibly overcome this limitation: as was shown for a system consisting of three spheres (80, 30, and 5 nm in diameter), we can expect a local intensity enhancement in air by a factor of 2300[18] to 250000,[23] depending on the precise alignment and positioning of the MNPs. Alas, the increased local intensity affects only a very small number of sensing molecules—this might result in a real challenge for recording scanned images, but it would be of great benefit for spectroscopic examinations of single molecules. A third route worth following is the usage of a more elaborated molecular framework instead of the rather simple alkanethiols used as Raman indicators here, in order to locally access information of, e.g., biochemical systems[34,35] or more complex heterostructures.[36]

Acknowledgment. The authors kindly appreciated funding through the Network of Excellence Plasmo-Nano-Devices hosted by the European Union in the sixth Framework Programme. The authors also whish to thank Tobias Otto for computer help.

Supporting Information Available: A video showing the electric field distribution of a two-particle field. This material is available free of charge via the Internet at http://pubs.acs.org.

References

(1) Novotny, L.; Hecht, B. *Principles of Nano-Optics*; Cambridge Unversity Press: Cambridge, New York, 2006.
(2) Lal, S.; Grady, N. K.; Goodrich, G. P.; Halas, N. J. *Nano Lett.* **2006**, *6*, 2338.
(3) Kühn, S.; Håkanson, U.; Rogobete, L.; Sandoghdar, V. *Phys. Rev. Lett.* **2006**, *97*, 017402.
(4) Domke, K. F.; Zhang, D.; Pettinger, B. *J. Am. Chem. Soc.* **2006**, *128*, 14721.
(5) Kalkbrenner, T.; Ramstein, M.; Mlynek, J.; Sandoghdar, V. *J. Microsc.* **2001** *202−1*, 72.
(6) Schneider, S. C.; Grafström, S.; Eng, L. M. *Phys. Rev. B* **2005**, *71*, 115418.
(7) Stöckle, R.; Suh, Y.; Deckert, V.; Zenobi, R. *Chem. Phys. Lett.* **2000**, *318*, 131.
(8) Demming, A. L.; Festy, F.; Richards, D. *J. Chem. Phys.* **2005**, *122*, 184716.
(9) Bouhelier, A.; Renger, J.; Beversluis, M.; Novotny, L. *J. Microsc.* **2003**, *210−3*, 220.
(10) Kottmann, J.; Martin, O. *Opt. Expr.* **2001**, *8*, 655.
(11) Blanco, L. A.; García de Abajo, F. J. *Phys. Rev. B* **2004**, *69*, 205414.
(12) ten Bloemendal, D.; Ghenuche, P.; Quidant, R.; Cormack, I. G.; Loza-Alvarez, P.; Badenes, G. *Plasmonics* **2006**, *1*, 41.
(13) Dahmen, C.; Schmidt, B.; von Plessen, G. *Nano Lett.* **2007**, *7*, 318.
(14) Su, K.-H.; Wei, Q.-H.; Zhang, X.; Mock, J. J.; Smith, D. R.; Schultz, S. *Nano Lett.* **2003**, *3*, 1087.
(15) Sönnichsen, C. *Plasmons in metal nanostructures*; Cuviller Verlag: Göttingen, 2001.

(16) Bosbach, J.; Hendrich, C.; Stietz, F.; Vartanyan, T.; Träger, F. *Phys. Rev. Lett.* **2002**, *89*, 257404.
(17) Renger, J.; Grafström, S.; Eng, L. M.; Deckert, V. *J. Opt. Soc. Am. A* **2004**, *21*, 1362.
(18) Renger, J. Excitation, Interaction, and Scattering of Localized and Propagating Surface Polaritons. Ph.D. Thesis, TU Dresden, 2006.
(19) Jiang, J.; Bosnick, K.; Maillard, M.; Brus, L. *J. Phys. Chem. B* **2003**, *107*, 9964.
(20) Svedberg, F.; Li, Z.; Xu, H.; Käll, M. *Nano Lett.* **2006**, *6*, 2639.
(21) Bergman, D. J.; Stockman, M. I. *Phys. Rev. Lett.* **2003**, *90*, 027402.
(22) Seidel, J.; Grafström, J.; Eng, L. M. *Phys. Rev. Lett.* **2005**, *94*, 177401.
(23) Li, K.; Stockman, M. I.; Bergman, D. J. *Phys. Rev. Lett.* **2003**, *91*, 227402.
(24) Karrai, K.; Grober, R. D. *Appl. Phys. Lett.* **1995**, *66*, 1842.
(25) Bryant, M. A.; Pemberton, J. E. *J. Am. Chem. Soc.* **1991**, *113*, 8284.
(26) Kudelski, A. *J. Raman Spectrosc.* **2003**, *11*, 853.
(27) Levin, C. S.; Janesko, B. G.; Bardhan, R.; Scuseria, G. E.; Hartgerink, J. D.; Halas, N. J. *Nano Lett.* **2006**, *6*, 2617.
(28) Schmidt, J. U.; Bergander, H.; Eng, L. M. *J. Appl. Phys.* **2000**, *87*, 3108.
(29) Hafner, C. *The Generalized Multipole Technique for Computational Electromagnetics*; Artech House: Norwood, MA, 1990.
(30) Hafner, C.; Bomholt, L. *The 3D Electrodynamic Wave Simulator*: Wiley: Chichester, U.K., 1993.
(31) Hafner, C. *Post-Modern Electromagnetics, Using Intelligent MaXwell Solvers*; Wiley: Chichester, U.K., 1999.
(32) Camillone, N.; Chidsey, C. E. D.; Liu, G.; Putvinski, T. M.; Scoles, G. *J. Chem. Phys.* **1991**, *94*, 8493.
(33) Novotny, L.; Grober, R. D.; Karrai, K. *Opt. Lett.* **2001**, *26*, 789.
(34) Pandey, P.; Singh, S. P.; Arya, S. K.; Gupta, V.; Datta, M.; Singh, S.; Malhotra, B. D. *Langmuir* **2007**, *23*, 3333.
(35) Govorov, A. O.; Carmeli, I. *Nano Lett.* **2007**, *7*, 620.
(36) Härtling, T.; Eng, L. M. *Appl. Phys. Lett.* **2005**, *87*, 142902.

NL070727M